Fundamental Research xxx (xxxx) xxx

Contents lists available at ScienceDirect

Fundamental Research

journal homepage: http://www.keaipublishing.com/en/journals/fundamental-research/

Article

Unveiling the critical role of TiO_2-supported atomically dispersed Cu species for enhanced photofixation of N_2 to nitrate

Dong Li[a,b], Yunxuan Zhao[a,*], Chao Zhou[a], Li-Ping Zhang[a,c], Junwang Tang[d], Tierui Zhang[a,b,*]

[a] Key Laboratory of Photochemical Conversion and Optoelectronic Materials, Technical Institute of Physics and Chemistry, Chinese Academy of Sciences, 100190 Beijing, China
[b] Center of Materials Science and Optoelectronics Engineering, University of Chinese Academy of Sciences, 100049 Beijing, China
[c] School of Future Technology, University of Chinese Academy of Sciences, 100049, Beijing, China
[d] Department of Chemical Engineering, University College London, WC1E 7JE, London, United Kingdom

ARTICLE INFO

Article history:
Received 30 March 2022
Received in revised form 19 May 2022
Accepted 23 May 2022
Available online xxx

Keywords:
N_2 photofixation
TiO_2
Nitrate photosynthesis
Cu species
NO_x intermediates

ABSTRACT

Nitrate products are widely used in manufacturing as crucial raw materials and fertilizers. The traditional nitrate synthesis process involves high energy consumption and emission, thereby opposing the goals of zero-carbon emission and green chemistry. Thus, a sustainable roadmap for nitrate synthesis that uses green energy input, clean N sources, and direct catalytic processes is urgently required (*e.g.*, developing a novel photosynthesis system). Here, we synthesized TiO_2-supported atomically dispersed Cu species for N_2 photofixation to nitrate in a flow reactor. The optimized photocatalyst yielded a high nitrate photosynthesis rate of 0.93 μmol h^{-1} and selectivity of ~90%, which is superior to most of the values reported thus far. Further, experimental results and *in-situ* investigations revealed that the atomically dispersed Cu sites in the as-designed sample significantly enhanced the separation and transfer efficiency of photogenerated carriers, adsorption and activation of reactants, and the formation of chemisorbed NO_x intermediates, thereby realizing the excellent photofixation of N_2 to nitrate.

1. Introduction

In addition to being used as chemical fibers, medicines and fertilizers in agriculture, as well as oxidants in explosives, nitrate products are essential for chemical analysis [1–5]. They are industrially produced by integrating the Haber–Bosch and Ostwald processes using noble metal catalysts under harsh conditions (15–25 MPa, 400–600 °C) [6–10]. Strict conditions and multi-step catalytic processes introduced during ammonia synthesis cause high energy consumption and emission, violating the current global zero-carbon emission goal. Theoretically, the use of clean N sources and green energy as alternatives may facilitate sustainable development. Crude saltpeter, atmospheric N_2, and ammonia have mainly been used as N sources. Among them, atmospheric N_2 is considered to be a promising alternative for ammonia because of its sustainability and accessibility. However, the sluggish dissociation of the N≡N bond of N_2 makes the industrial N_2 activation technique demanding and energy-intensive, which accelerates the flourish of the mild N_2 activation technique [11–14]. In addition, efficient non-precious-metal-based catalysts must be explored to replace expensive noble metals. At present, the simultaneous achievement of high-efficiency and sustainable nitrate synthesis over non-precious metal catalysts is considerably challenging.

N_2 fixation to nitrate is a common oxidation reaction [5]. Hence, the application of photocatalysis, which is widely studied as an advanced oxidation technology, may be beneficial for this process. TiO_2, which is a commonly used photocatalyst, exhibits excellent oxidation properties that may benefit the photofixation of N_2 to nitrate under ambient conditions. Recently, several studies have shown that TiO_2-based photocatalysts could photofix N_2 to nitrate or nitrite [10–16]. However, the poor performance of such photocatalysts makes them unsuitable for industrial use. The reaction involves the following two obstacles: i) adsorption and activation of gaseous reactant molecules, particularly inert molecular N_2, and ii) efficient charge transfer for the subsequent bonding process of N_2 and O_2. Extensive research has been conducted to overcome these obstacles and enhance the yield. Metal-doping strategies that can introduce other active sites and improve photogenerated charge transfer have been extensively applied in photocatalysis [17,18]. Among non-precious metals, metallic Cu, which can act as a catalytic center or promoter, has drawn particular attention for N_2 photofixation. Moreover, Cu-catalyzed cross-coupling reactions inspired us to consider

* Corresponding authors.
E-mail addresses: yunxuan@mail.ipc.ac.cn (Y. Zhao), tierui@mail.ipc.ac.cn (T. Zhang).

https://doi.org/10.1016/j.fmre.2022.05.025

the possibility of using Cu species for the efficient coupling of N_2 and O_2 [19], which may benefit the formation of N–O bonds for nitrate photosynthesis. Therefore, constructing Cu-doped TiO_2 that can expose abundant Cu species is expected to be an advanced strategy for facilitating charge transfer efficiency, as well as the adsorption and activation of reactants to promote nitrate formation.

Herein, we prepared TiO_2-supported atomically dispersed Cu species for N_2 photofixation to nitrate in a flow reactor. Results indicated that 1 mol% Cu-doped TiO_2 (herein denoted as 1% Cu/TiO_2) exhibited a high nitrate photosynthesis rate of 0.93 μmol h^{-1}, outperforming most photocatalysts reported to date. Detailed characterizations indicated that the Cu species were atomically dispersed in TiO_2 and produced excellent active sites during use. *In-situ* diffuse reflectance infrared Fourier transform spectroscopy (DRIFTS) confirmed that Cu species acted as active sites to control the reaction pathway to nitrate through the NO_x intermediates. Subsequent measurements (*i.e.*, temperature-programmed desorption measurements and kinetic behaviors of photogenerated carriers) revealed that the Cu species enhanced the separation and transfer efficiency of photogenerated carriers and promoted the adsorption and activation of N_2 and O_2. Thus, the photofixation of N_2 to nitrate exhibited excellent performance.

2. Materials and methods

2.1. Preparation of photocatalysts

TiO_2 photocatalysts doped with different amounts of Cu were synthesized by using a facile solvothermal method [20] (denoted as x% Cu/TiO_2, where $x = 100 \times mol_{Cu} / mol_{TiO2}$, x = 0, 0.5, 1, 3, 6). Typically, a certain amount of $CuCl_2 \cdot 2H_2O$, 1.2 mL of hydrofluoric acid, and 10 mL of tetrabutyl titanate were added to 40 mL of anhydrous ethanol. After being stirred, the mixed solution was transferred to a Teflon-lined stainless-steel autoclave and heated at 180°C for 12 h. The final product was washed with ultrapure water and dried overnight at 60 °C. Other metal-doped TiO_2 samples, except for the corresponding metal chloride salts, were prepared by using a synthetic method similar to that for Cu/TiO_2.

2.2. Photocatalytic tests

The photocatalytic N_2 fixation reaction was conducted in a self-built reaction system that contained a customized quartz flow reactor and an absorption cell filled with 10 mL of ultrapure water. The photocatalyst (100 mg) was dispersed in 50 mL of ultrapure water (18.2 MΩ), sonicated for 1 h and then filtered through a microfiltration membrane (hydrophilic, bore diameter: 0.2 μm). After being filtered, the photocatalysts were further washed with 200 mL of ultrapure water, transferred to a clean oven, and dried overnight at 60°C. The freshly cleaned photocatalysts with the membrane were transferred to a flow reactor (diameter 23 mm). Subsequently, the reaction gas (N_2:O_2 = 4:1) penetrated the photocatalysts from top to bottom at a flow rate of 8 mL min^{-1}. After 30 min of pre-ventilation, a monochromatic light source (λ = 365 nm) was introduced by using a PLS-LED100B lamp (Beijing PerfectLight) for photocatalytic N_2 conversion. After irradiation, the products were collected and identified by employing an ion chromatography (930 compact IC Flex, Metrohm). $^{14}N_2$ and $^{15}N_2$ were used to conduct an isotopic tracing test in a batch kettle reactor and the product was analyzed directly by using liquid chromatography-high resolution mass spectrometry (LC-HRMS) [21].

2.3. In-situ *DRIFTS measurements*

In-situ DRIFTS was conducted to monitor the intermediates formed during photocatalytic N_2 fixation to nitrate under ambient temperature and pressure conditions. *In-situ* DRIFTS data were collected every minute at a resolution of 4 cm^{-1}. A Vector 70v (Brucker) spectrophotometer equipped with a liquid-N_2 cooled detector and a custom-built *in-situ* diffuse reflectance cell was used for the DRIFTS studies. A 365 nm LED (PLS-LED100B) light was used as the light source. For each subsequent test, 50 mg of the catalyst was compacted into the reaction cell. Subsequently, a feeding gas (N_2:O_2 or Ar) was introduced into a reactor at a flow rate of 8 mL min^{-1} to achieve an experimental atmosphere. Finally, the 365 nm LED light was turned on and *in-situ* DRIFTS data were collected as a function of the irradiation time using an MCT detector.

3. Results and discussion

3.1. Synthesis and characterization of photocatalysts

The as-designed Cu/TiO_2 photocatalysts were successfully synthesized by using a facile solvothermal method [20] and directly confirmed by the corresponding X-ray diffraction (XRD) patterns (Fig. S1). No distinct peaks corresponding to the Cu-containing matter (CuO_x or Cu metal particles) were observed in any of Cu/TiO_2 samples, indicating that Cu species were highly dispersed in Cu/TiO_2. Ultraviolet-Visible diffuse reflectance spectroscopy showed intensified absorbance ranging over 400–800 nm with an increasing Cu content in Cu/TiO_2 (Fig. S2), which could be attributed to the absorption of Cu species [22], providing latent evidence for the successful introduction of Cu species into TiO_2. Moreover, transmission electron microscopy (TEM) and high-resolution transmission electron microscopy (HRTEM) were conducted, further revealing that the as-prepared 0% Cu/TiO_2 had a size of 20–30 nm (Fig. S3). After Cu species were introduced, the TEM image of the synthesized Cu/TiO_2 sample (1% Cu/TiO_2 was taken as a representative example; Fig. 1a) indicated that the sample was approximately the same size (20–30 nm) as 0% Cu/TiO_2. The Moiré fringe spacing of 0.35 nm in the HRTEM image (Fig. 1b) could be attributed to the (101) plane of anatase TiO_2; this is in good agreement with the aforementioned XRD findings. TEM and HRTEM images of 1% Cu/TiO_2 also indicated the absence of Cu nanoparticles whereas uniformly dispersed Cu element was detected by applying energy dispersive spectroscopy (EDS) elemental mapping (Fig. 1c). This provides an auxiliary note for the mono-dispersion of Cu species.

The mono-dispersion of Cu species was further identified by performing X-ray absorption fine structure (XAFS) spectroscopy. The Fourier transform k^3-weighted extended XAFS (EXAFS) spectra of 1% Cu/TiO_2 and standard Cu samples (Cu foil, Cu_2O and CuO) at Cu k-edge are presented in Fig. 1d. The 1% Cu/TiO_2 displays its highest absorbance at ~1.5 Å (the contribution of Cu-O in CuO [23–26]), and no obvious peaks appear at ~2.25 Å (the contribution of Cu-Cu [23–26]), suggesting the presence of Cu coordinated to O atoms and the absence of Cu-Cu shell in 1% Cu/TiO_2. These observations clearly affirm that Cu atoms were mono-dispersed in 1% Cu/TiO_2. Further, the mono-dispersion of the Cu atoms was visualized by conducting wavelet transform analysis. As shown in Fig. 1e, f, the discrepancy between the intensity maximum in the wavelet transform image of 1% Cu/TiO_2 and the Cu foil (~1.5 Å vs. ~2.25 Å) is consistent with the results of EXAFS, confirming the mono-dispersion of Cu in 1% Cu/TiO_2. Additionally, the horizontal axis of the wavelet transform plot shows the wave vector (k), which is the key to distinguishing the different types of coordination atoms. Compared with that of the Cu foil (6–9 $Å^{-1}$), the strongest oscillation or intensity maximum of 1% Cu/TiO_2 in k space shifts to a lower k space (4–7 $Å^{-1}$), implying that Cu is coordinated by atoms with smaller atomic numbers. As described earlier, the successful preparation of TiO_2-supported atomically dispersed Cu species provides excellent active sites for the conversion of N_2 to nitrate. The results are confirmed and discussed in detail as follows.

3.2. Photofixation of N_2 to nitrate

The photofixation of N_2 to nitrate was performed in a flow reactor under an irradiation with 365 nm LED light (Figs. 2a and S4). The

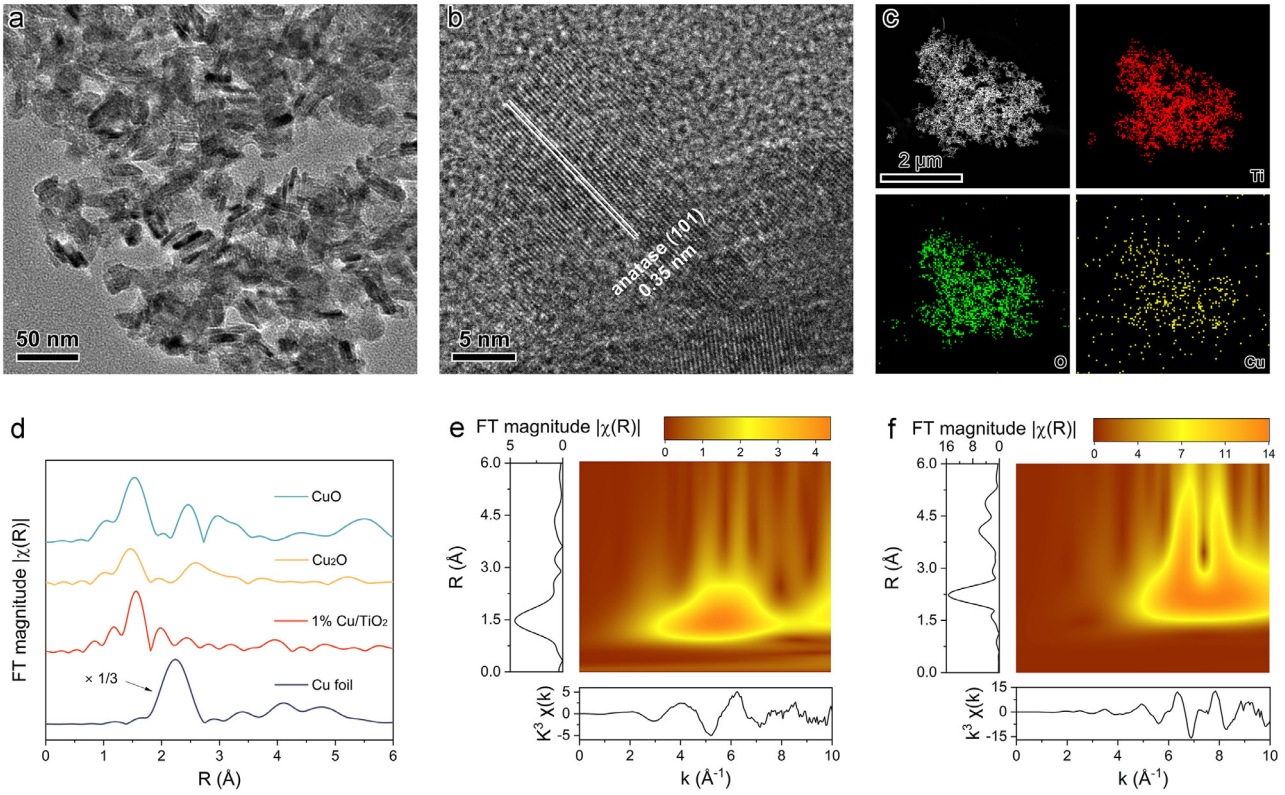

Fig. 1. Structural characterizations of as-designed Cu/TiO_2. (a) TEM, (b) HRTEM images and (c) EDS elemental mapping of 1% Cu/TiO_2. (d) k^3-weighted Fourier transform of the EXAFS spectra for 1% Cu/TiO_2 and standard Cu samples at Cu k-edge. Wavelet transform analysis from EXAFS of (e) 1% Cu/TiO_2 and (f) Cu foil.

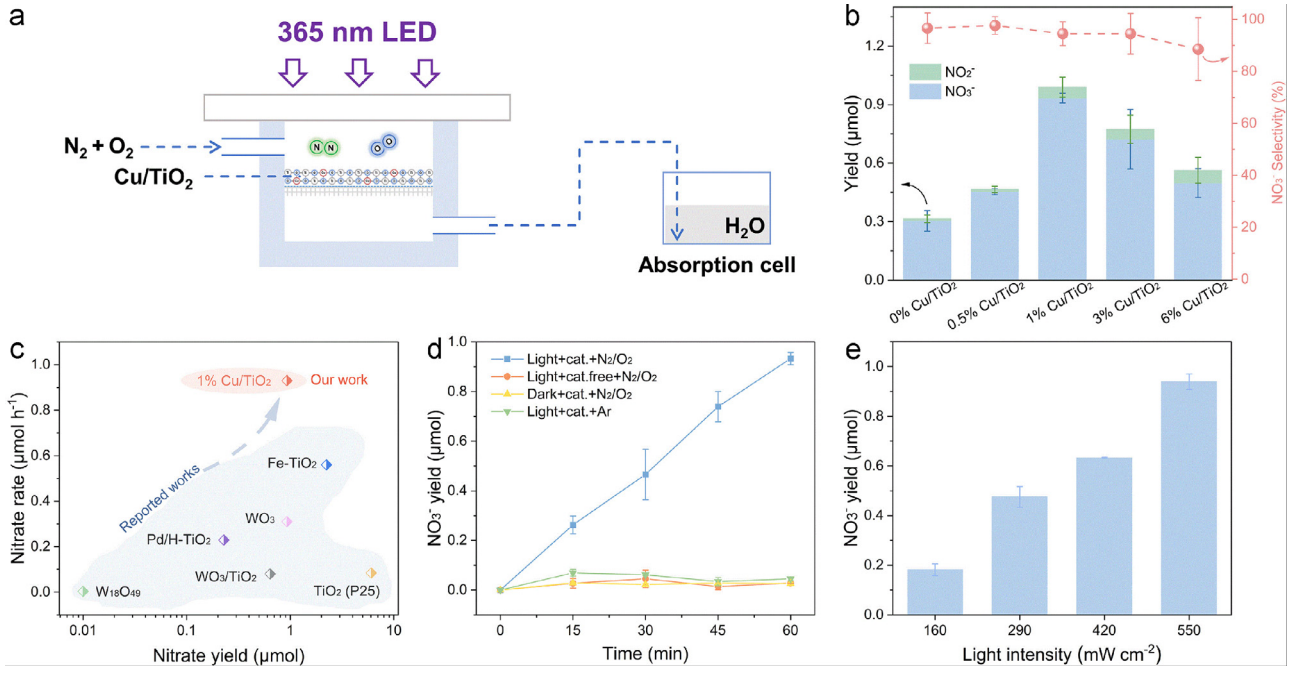

Fig. 2. Evolution of the photocatalytic performance of Cu/TiO_2 in a flow cell. (a) Schematic illustration of the reaction system. (b) N_2 photofixation performance of x% Cu/TiO_2 under 550 mW cm^{-2} of irradiation for 1 h. (c) Comparison between the performance of 1% Cu/TiO_2 and reported photocatalysts [5,10,15,16,27,28]. (d) NO_3^- yield of 1% Cu/TiO_2 under different time and conditions (dark or light; with or without catalyst; different reactants: N_2:O_2 or Ar). (e) NO_3^- yield under different irradiation intensities for 1 h.

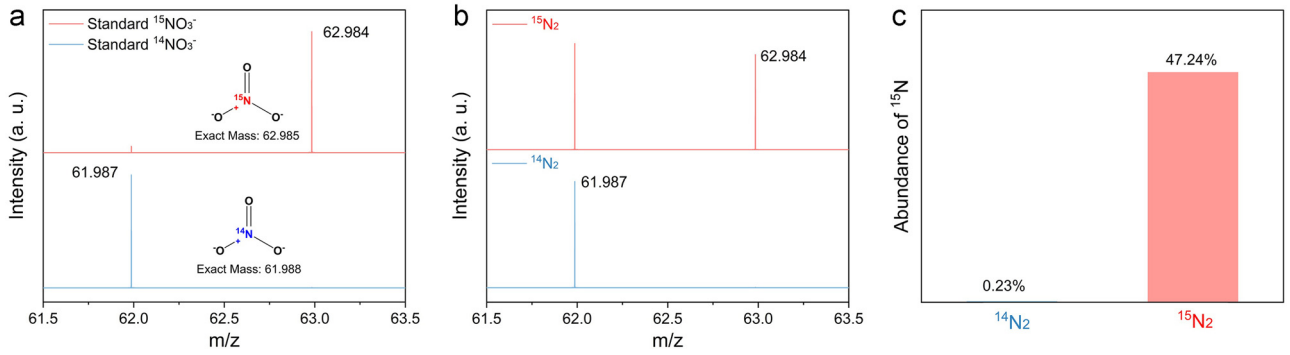

Fig. 3. Isotope-labelling measurement results. HRMS data of (a) standard nitrate samples and (b) produced nitrate with pure $^{14}N_2$ and additional $^{15}N_2$ as reactants. (c) Calculated ^{15}N abundance of produced NO_3^- under different feeding gas.

feeding gas, a mixture of N_2 and O_2 (N_2:O_2 = 4:1), was blown into the reactor at a flow rate of 8 mL·min^{-1}. After irradiation, the related products were collected and identified by using ion chromatography to quantify the generated nitrate or nitrite (the standards are shown in Fig. S5, and Table S1, 2). As expected, the results shown in Fig. S6 suggested that all of the different metal-doped TiO_2 photocatalysts are active for N_2 photofixation to nitrate. The Cu-doped TiO_2 conveyed the highest yield of nitrate with considerable selectivity (94.49%) compared with other photocatalysts. Thus, the corresponding performances for N_2 photofixation to nitrate of Cu-doped TiO_2 with different Cu amounts (x% Cu/TiO_2) were further studied. As shown in Fig. 2b, photocatalysts performed the detectable yield of nitrate following the order: 1% Cu/TiO_2 (0.93 μmol h^{-1}) > 3% Cu/TiO_2 (0.72 μmol h^{-1}) > 6% Cu/TiO_2 (0.50 μmol h^{-1}) > 0.5% Cu/TiO_2 (0.45 μmol h^{-1}) > 0% Cu/TiO_2 (0.30 μmol h^{-1}), together with high nitrate selectivity (≥ 90%). Among the x% Cu/TiO_2 samples, 1% Cu/TiO_2 exhibited the highest yield of nitrate with the threefold enhancement factor of 0% Cu/TiO_2, which is superior to most of the reported photocatalysts (Fig. 2c) [5–28]. The excellent photogenerated nitrate rate and structure of 1% Cu/TiO_2 can be maintained and stabilized after five cycle tests (Figs. S7, S8). Increasing the doping amount of Cu to 3% and 6% resulted in a decrease in activity from 0.72 to 0.50 μmol h^{-1}, which may be caused by the significantly reduced oxidation ability of the Cu/TiO_2 samples (Fig. S9). Moreover, a series of control experiments (*e.g.*, in pure Ar, without light or a photocatalyst) showed little nitrate evolution (Figs. 2d and S10). Hence, a photocatalytic system co-containing photocatalysts (1% Cu/TiO_2), light irradiation, and N_2:O_2 gas mixture as reactants could present an outstanding performance that increased over time. The aforementioned control experiments emphasized the indispensable role that photocatalyst, light irradiation, and N_2:O_2 as reactants play in nitrate photosynthesis. Further, the relationship between the nitrate yield and irradiated light intensity was investigated in detail (Fig. 2e), and the corresponding original ion chromatograms are presented in Fig. S11. The detected nitrate yield followed the trend of the irradiation intensity, suggesting that the fixation of N_2 to nitrate is a photocatalytic process.

3.3. Identification of the N source in produced nitrate

To further confirm that the produced nitrate originated from N_2, ^{15}N-labeled isotope-tracing experiments were conducted with the collected products measured by using LC-HRMS. First, we identified the mass-to-charge ratio (m/z) of the standard nitrate samples labeled with ^{14}N and ^{15}N ($^{14}NO_3^-$ and $^{15}NO_3^-$). In Fig. 3a, the HRMS data of the standard nitrate samples displayed that the m/z values of $^{14}NO_3^-$ and $^{15}NO_3^-$ are 61.987 and 62.984, respectively. These results are consistent with the corresponding exact masses ($^{14}NO_3^-$: 61.988 g/mol and $^{15}NO_3^-$: 62.985 g/mol). Then, the photofixation of N_2 to nitrate using $^{14}N_2$ as N source was performed for comparison (Fig. 3b), and a peak at m/z 61.987 was detected, qualitatively indicating the generation of nitrate ($^{14}NO_3^-$). When $^{15}N_2$ was additionally bubbled into the reactor, another peak at m/z 62.984 appeared, which was assigned to $^{15}NO_3^-$. This result suggests that the produced nitrate could have originated from $^{15}N_2$. The calculated abundance of $^{15}NO_3^-$ detected in the ^{15}N-isotope-tracing experiment was 47.24% (Fig. 3c), which was significantly higher than the abundance of the product generated using $^{14}N_2$ as the feeding gas (0.23%) or the natural ^{15}N abundance (~0.34%) [9–29]. The presented isotope-tracing experiments confirmed that photogenerated nitrate could originate from atmospheric N_2.

3.4. Investigation of reaction intermediates and behaviors of photoinduced carriers

In-situ DRIFTS was conducted to monitor the intermediates formed during photocatalytic N_2 fixation under ambient temperature and pressure conditions. For the 1% Cu/TiO_2 photocatalyst with a N_2:O_2 mixture as the feeding gas, an obvious peak (2121 cm^{-1}) appeared near CO_2, assigned to the vibrations of NO_x intermediates (NO_2^+, NO^+, or $NO^{\delta+}$) adsorbed at the Cu sites after irradiation [30–33]. This peak increased along with the irradiation time (Figs. S12 and 4a). The enhanced NO_x intermediates strongly agree with the evolution trend of nitrate with the prolonged irradiation time, as depicted in Fig. 2d. This result indicated that Cu species acting as active sites may undertake the reaction pathway to produce nitrate through the NO_x intermediates. Further, when the feeding gas was turned into single-component Ar, N_2 or O_2 molecules for comparison, the peak at 2121 cm^{-1} was not observed after 1 h of continuous irradiation (Fig. S13); this further indicated the indispensability of co-existing N_2 and O_2 as reactants and the origin of the N and O sources in the produced nitrate. More importantly, the 0% Cu/TiO_2 photocatalyst without Cu species did not exhibit any peaks at ~2121 cm^{-1} in the photofixation process of N_2 and O_2 mixtures. The comparative results also provided convincing evidence that atomically dispersed Cu species act as efficient active sites in Cu/TiO_2 to benefit the formation of NO_x intermediate species, thus promoting high-efficiency nitrate photosynthesis through the NO_x intermediate pathway. Furthermore, the discrepancy between the adsorption and activation of 0% Cu/TiO_2 and 1% Cu/TiO_2 was further studied by performing N_2- and O_2-temperature-programmed desorption (N_2-TPD and O_2-TPD) measurements. As shown in Fig. 4b, 1% Cu/TiO_2 exhibited three enhanced N_2-desorption peaks at 213, 250 and 307 °C relative to those of 0% Cu/TiO_2, and these are attributed to physically adsorbed and chemisorbed N_2 onto the catalyst surface [34]. The same tendency can be observed in O_2-TPD (Fig. 4c), indicating the enhanced adsorption and activation of O_2. The co-enhanced adsorption and activation of N_2 and O_2 by 1% Cu/TiO_2 are likely responsible for the outstanding nitrate photosynthesis activity.

In addition to the enhanced adsorption and activation of reactants, the charge transfer behaviors could play an indispensable role in the enhanced performance [35–39]. To investigate the photoinduced charge

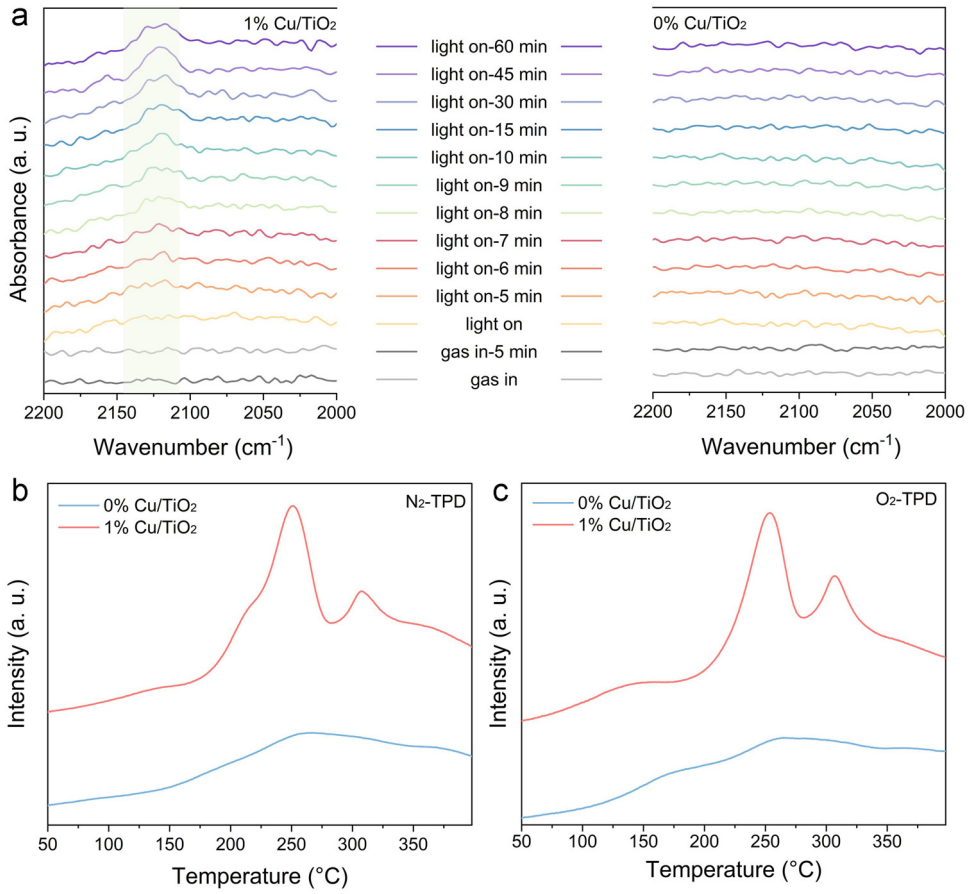

Fig. 4. *In-situ* characterization and TPD responses. (a) *In-situ* DRIFTS measurements of 0% Cu/TiO_2 and 1% Cu/TiO_2 with N_2:O_2 mixture as the feeding gas. (b) N_2-TPD and (c) O_2-TPD measurements of 0% Cu/TiO_2 and 1% Cu/TiO_2.

transfer in 1% Cu/TiO_2, we performed the Mott–Schottky measurements of 0% Cu/TiO_2 and 1% Cu/TiO_2 (Figs. 5a and S14). The Mott–Schottky plots revealed that both 0% Cu/TiO_2 and 1% Cu/TiO_2 are n-type semiconductors. The charge distribution at the semiconductor is usually determined based on the Mott–Schottky relationship between electrode capacitance C and electrode potential E, as shown in the following equation [40,41]:

$$\frac{1}{C^2} = \frac{2}{\varepsilon\varepsilon_0 e N_D}\left(E - E_{fb} - \frac{KT}{e}\right)$$

where e is the electron charge, the dielectric constant (ε) of anatase TiO_2 is 55 [42], ε_0 is the vacuum permittivity (8.854×10^{-14} F/cm), Boltzmann constant K is 1.38×10^{23} J/K, and T and E_{fb} are the absolute temperature and flat band potential, respectively [40,41]. The fitted relationship between $1/C^2$ and the potential (E), presented in Fig. 5a, is used to conclude that the Mott–Schottky curve slopes of 0% Cu/TiO_2 and 1% Cu/TiO_2 are 69.08×10^9 $cm^4/(F^2\ V)$ and 38.90×10^9 $cm^4/(F^2\ V)$, respectively. Thus, the donor density (N_D) of 0% Cu/TiO_2 and 1% Cu/TiO_2 (3.72×10^{19} cm^{-3} *vs.* 6.60×10^{19} cm^{-3}, presented in Fig. 5b) can be calculated by applying the aforementioned equation, and both values are consistent with the reported value (10^{16}–10^{20} cm^{-3}) [42–44]. The difference in N_D indicated that Cu species increase the inherent charge density of 1% Cu/TiO_2 by ~1.77 times compared with that of 0% Cu/TiO_2, and this may provide more photogenerated charges for the subsequent bonding process of N_2 and O_2 to form NO_x intermediates and nitrate. Further, the corresponding kinetic behaviors of photogenerated charges were analyzed by employing photocurrent measurements, electrochemical impedance spectra, photoluminescence spectra and fluorescence dynamic decay curves (Figs. 5c-e and S15). The photocurrent measurements revealed that TiO_2 after doping with Cu species shows an enhanced current density under irradiation, indicating improved charge separation and transfer efficiency [45,46]. The trend of enhanced carrier separation and migration is also in accordance with the results obtained from the analysis of electrochemical impedance spectra owing to the smaller arc radius (Fig. 5d). As presented in Figs. S15, 5e, and Table S3, the charge separation efficiency in 1% Cu/TiO_2 caused a lower radiative relaxation and prolonged lifetime (8.79 ns) than that of 0% Cu/TiO_2 (4.95 ns), suggesting that more charges are likely transferred to the surface of the photocatalyst [36–38]. In summary, 1% Cu/TiO_2 exhibited efficient charge separation and migration efficiencies, which may jointly contribute to the considerable N_2 photofixation ability of 1% Cu/TiO_2.

4. Conclusion

We successfully achieved the high-efficiency N_2 photofixation to nitrate in a flow reactor, with an outstanding nitrate photosynthesis rate of 0.93 μmol h^{-1}, which is higher than most of the results reported to date. The introduction of Cu species as dopants in TiO_2 enhanced the charge separation and transfer properties. Meanwhile, the surface Cu species acted as active sites to promote the adsorption and activation of reactants (N_2 and O_2), and further generate NO_x intermediates. Thus, the photocatalytic activity for the N_2 photofixation process through the NO_x intermediate pathway was synergistically boosted. Our findings are expected to be helpful in the development and design of high-performance photocatalysts containing low-cost metal sites for N_2 photofixation and other challenging chemical reactions.

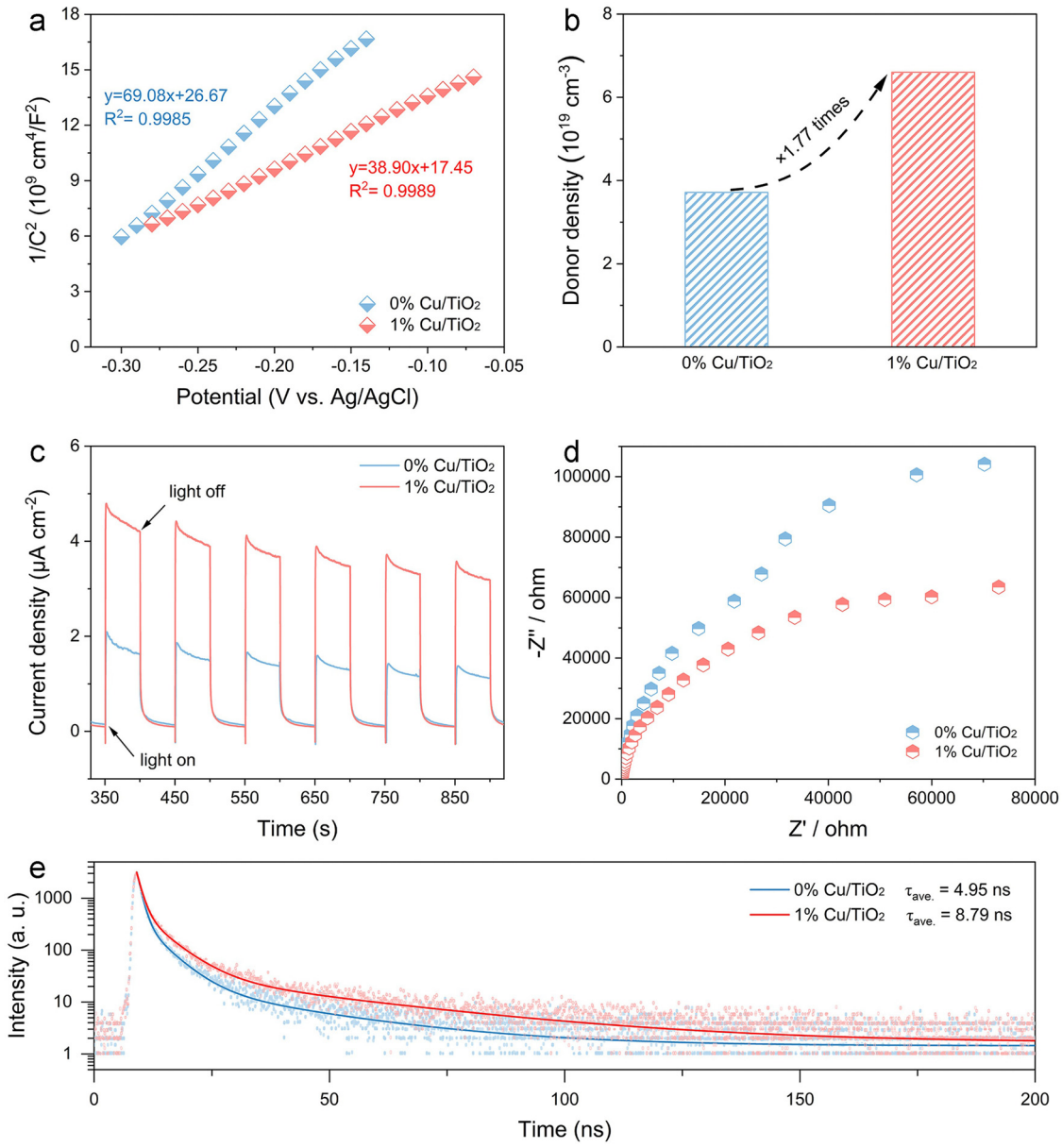

Fig. 5. Dynamic behaviors of photoinduced carriers. (a) Fitted Mott–Schottky plots, (b) calculated donor density, (c) photocurrent measurements, (d) electrochemical impedance spectra under irradiation, and (e) time-resolved fluorescence dynamic decay curves of 0% Cu/TiO_2 and 1% Cu/TiO_2 (excitation: 375 nm; emission: 440 nm).

Declaration of Competing Interest

The authors declared that they have no conflicts of interest in this work

Acknowledgments

The authors are grateful for financial support from the National Key Projects for Fundamental Research and Development of China (Grant No. 2018YFB1502002), the National Natural Science Foundation of China (Grants No. 51825205, 52120105002, 52072382, 22102202, and 22088102), the Beijing Natural Science Foundation (Grant No. 2191002), the DNL Cooperation Fund, CAS (Grant No. DNL202016), the CAS Project for Young Scientists in Basic Research (Grant No. YSBR-004), the Strategic Priority Research Program of the Chinese Academy of Sciences (Grant No. XDB17000000), and the China Postdoctoral Science Foundation (Grant No. BX2021323).

Supplementary materials

Supplementary material associated with this article can be found, in the online version, at doi:10.1016/j.fmre.2022.05.025.

References

[1] J.G. Chen, R.M. Crooks, L.C. Seefeldt, et al., Beyond fossil fuel-driven nitrogen transformations, Science 360 (2018) eaar6611.
[2] C. Dai, Y. Sun, G. Chen, et al., Electrochemical oxidation of nitrogen towards direct nitrate production on spinel oxides, Angew. Chem. Int. Ed. 59 (2020) 9418–9422.
[3] S. Han, C. Wang, Y. Wang, et al., Electrosynthesis of nitrate via the oxidation of nitrogen on tensile-strained palladium porous nanosheets, Angew. Chem. Int. Ed 133 (2021) 4524–4528.
[4] Y. Wang, Y. Yu, R. Jia, et al., Electrochemical synthesis of nitric acid from air and ammonia through waste utilization, Natl. Sci. Rev. 6 (2019) 730–738.
[5] Y. Liu, M. Cheng, Z. He, et al., Pothole-rich ultrathin WO3 nanosheets that trigger N N bond activation of nitrogen for direct nitrate photosynthesis, Angew. Chem. Int. Ed. 58 (2019) 731–735.
[6] S.Z. Andersen, V. Čolić, S. Yang, et al., A rigorous electrochemical ammonia synthesis protocol with quantitative isotope measurements, Nature 570 (2019) 504–508.

[7] T. Kandemir, M.E. Schuster, A. Senyshyn, et al., The Haber-Bosch process revisited: on the real structure and stability of "ammonia iron" under working conditions, Angew. Chem. Int. Ed. 52 (2013) 12723–12726.
[8] L. Li, C. Tang, X. Cui, et al., Efficient nitrogen fixation to ammonia through integration of plasma oxidation with electrocatalytic reduction, Angew. Chem. Int. Ed. 133 (2021) 14250–14256.
[9] T. Li, S. Han, C. Wang, et al., Ru-doped Pd nanoparticles for nitrogen electrooxidation to nitrate, ACS Catal. 11 (2021) 14032–14037.
[10] S.-J. Yuan, J.-J. Chen, Z.-Q. Lin, et al., Nitrate formation from atmospheric nitrogen and oxygen photocatalysed by nano-sized titanium dioxide, Nat. Commun. 4 (2013) 2249.
[11] C. Li, T. Wang, Z.J. Zhao, et al., Promoted fixation of molecular nitrogen with surface oxygen vacancies on plasmon-enhanced TiO_2 photoelectrodes, Angew. Chem. Int. Ed. 57 (2018) 5278–5282.
[12] H. Li, J. Shang, Z. Ai, et al., Efficient visible light nitrogen fixation with BiOBr nanosheets of oxygen vacancies on the exposed {001} facets, J. Am. Chem. Soc. 137 (2015) 6393–6399.
[13] S. Wang, X. Hai, X. Ding, et al., Light-switchable oxygen vacancies in ultrafine Bi_5O_7Br nanotubes for boosting solar-driven nitrogen fixation in pure water, Adv. Mater. 29 (2017) 1701774.
[14] D. Zhu, L. Zhang, R.E. Ruther, et al., Photo-illuminated diamond as a solid-state source of solvated electrons in water for nitrogen reduction, Nat. Mater. 12 (2013) 836–841.
[15] J. Yang, H. Bai, Y. Guo, et al., Photodriven disproportionation of nitrogen and its change to reductive nitrogen photofixation, Angew. Chem. Int. Ed. 60 (2021) 927–936.
[16] Y. Yu, C. Wang, Y. Yu, et al., A nitrogen fixation strategy to synthesize NO via the thermally assisted photocatalytic conversion of air, J. Mater. Chem. A 8 (2020) 19623–19630.
[17] L. An, H. Onishi, Electron-hole recombination controlled by metal doping sites in $NaTaO_3$ photocatalysts, ACS Catal. 5 (2015) 3196–3206.
[18] D. Dvoranová, V. Brezová, M. Mazúr, et al., Investigations of metal-doped titanium dioxide photocatalysts, Appl. Catal., B 37 (2002) 91–105.
[19] S. Bhunia, G.G. Pawar, S.V. Kumar, et al., Selected copper-based reactions for C-N, C-O, C-S, and C-C bond formation, Angew. Chem. Int. Ed. 56 (2017) 16136–16179.
[20] Y. Zhao, Y. Zhao, R. Shi, et al., Tuning oxygen vacancies in ultrathin TiO_2 nanosheets to boost photocatalytic nitrogen fixation up to 700 nm, Adv. Mater. 31 (2019) 1806482.
[21] W.S. Jobgen, S.C. Jobgen, H. Li, et al., Analysis of nitrite and nitrate in biological samples using high-performance liquid chromatography, J. Chromatogr. B 851 (2007) 71–82.
[22] G. Colón, M. Maicu, M.C. Hidalgo, et al., Cu-doped TiO_2 systems with improved photocatalytic activity, Appl. Catal., B 67 (2006) 41–51.
[23] J. Wang, T. Heil, B. Zhu, et al., A single Cu-center containing enzyme-mimic enabling full photosynthesis under CO_2 reduction, ACS Nano 14 (2020) 8584–8593.
[24] X. Xiao, Y. Gao, L. Zhang, et al., A promoted charge separation/transfer system from Cu single atoms and C_3N_4 layers for efficient photocatalysis, Adv. Mater. 32 (2020) e2003082.
[25] G. Wang, C.T. He, R. Huang, et al., Photoinduction of Cu single atoms decorated on UiO-66-NH_2 for enhanced photocatalytic reduction of CO_2 to liquid fuels, J. Am. Chem. Soc. 142 (2020) 19339–19345.
[26] B.H. Lee, S. Park, M. Kim, et al., Reversible and cooperative photoactivation of single-atom Cu/TiO_2 photocatalysts, Nat. Mater. 18 (2019) 620–626.
[27] X. Zhang, R. Shi, Z. Li, et al., Photothermal-assisted photocatalytic nitrogen oxidation to nitric acid on palladium-decorated titanium oxide, Adv. Energy Mater. (2022) 2103740.
[28] W. Ren, Z. Mei, S. Zheng, et al., Wavelength-dependent solar N_2 fixation into ammonia and nitrate in pure water, Research (2020) 3750314 2020.
[29] A. Mariotti, Natural ^{15}N abundance measurements and atmospheric nitrogen standard calibration, Nature 311 (1984) 251–252.
[30] A.W. Aylor, S.C. Larsen, J.A. Reimer, et al., An infrared study of NO decomposition over Cu-ZSM-5, J. Catal. 157 (1995) 592–602.
[31] K.I. Hadjiivanov, Identification of neutral and charged N_xO_y surface species by IR spectroscopy, Catal. Rev. 42 (2000) 71–144.
[32] J. Valyon, W.K. Hall, Studies of the surface species formed from nitric oxide on copper zeolites, J. Phys. Chem. 97 (1993) 1204–1212.
[33] J.C. Wu, Y.-T. Cheng, In situ FTIR study of photocatalytic NO reaction on photocatalysts under UV irradiation, J. Catal. 237 (2006) 393–404.
[34] X. Bian, Y. Zhao, S. Zhang, et al., Enhancing the supply of activated hydrogen to promote photocatalytic nitrogen fixation, ACS Mater. Lett. 3 (2021) 1521–1527.
[35] X. Cao, Z. Chen, R. Lin, et al., A photochromic composite with enhanced carrier separation for the photocatalytic activation of benzylic C-H bonds in toluene, Nat. Catal. 1 (2018) 704–710.
[36] S. Fukuzumi, K. Ohkubo, T. Suenobu, Long-lived charge separation and applications in artificial photosynthesis, Acc. Chem. Res. 47 (2014) 1455–1464.
[37] Z. Li, Y. Pi, D. Xu, et al., Utilization of MoS_2 and graphene to enhance the photocatalytic activity of Cu_2O for oxidative C-C bond formation, Appl. Catal., B 213 (2017) 1–8.
[38] P. Bai, X. Tong, Y. Gao, et al., Visible light-driven selective carbon–carbon bond formation for the production of vicinal diols, Sustain. Energ Fuels. 4 (2020) 5488–5492.
[39] H.H. Mohamed, D.W. Bahnemann, The role of electron transfer in photocatalysis: fact and fictions, Appl. Catal., B 128 (2012) 91–104.
[40] H. Guo, B. Lu, J. Luo, Study on passivation and erosion-enhanced corrosion resistance by Mott-Schottky analysis, Electrochim. Acta 52 (2006) 1108–1116.
[41] A. Fattah-Alhosseini, Passivity of AISI 321 stainless steel in 0.5 M H_2SO_4 solution studied by Mott-Schottky analysis in conjunction with the point defect model, Arabian J. Chem. 9 (2016) S1342–S1348.
[42] C.S. Enache, J. Schoonman, R.V. Krol, The photoresponse of iron-and carbon-doped TiO_2 (anatase) photoelectrodes, J. Electroceram. 13 (2004) 177–182.
[43] E.-J. Lee, S.-I. Pyun, Analysis of nonlinear Mott-Schottky plots obtained from anodically passivating amorphous and polycrystalline TiO_2 films, J. Appl. Electrochem. 22 (1992) 156–160.
[44] M.C. Sellers, E.G. Seebauer, Measurement method for carrier concentration in TiO_2 via the Mott-Schottky approach, Thin Solid Films. 519 (2011) 2103–2110.
[45] X. Liu, Z. Hao, H. Wang, et al., Enhanced localized dipole of Pt-Au single-site catalyst for solar water splitting, Proc. Natl. Acad. Sci. U. S. A. 119 (2022) e2119723119.
[46] Y. Wang, X. Shang, J. Shen, et al., Direct and indirect Z-scheme heterostructure-coupled photosystem enabling cooperation of CO_2 reduction and H_2O oxidation, Nat. Commun. 11 (2020) 3043.

Dong Li received his B. S. degree in Materials Chemistry from the China University of Petroleum (East China) in 2019. He is now a Ph.D. candidate in Materials Science at the Technical Institute of Physics and Chemistry, Chinese Academy of Sciences. His research interests focus on the design and synthesis of nanomaterials for photocatalytic nitrogen fixation.

Tierui Zhang is a full professor at the Technical Institute of Physics and Chemistry, Chinese Academy of Sciences. He obtained his Ph.D. degree in Chemistry in 2003 at Jilin University, China. He then worked as a postdoctoral researcher in the labs of Prof. Markus Antonietti, Prof. Charl F. J. Faul, Prof. Hicham Fenniri, Prof. Z. Ryan Tian, Prof, Yadong Yin, and Prof. Yushan Yan. His current scientific interests focus on catalyst nanomaterials for energy conversion.